AIAA JOURNAL
Vol. 36, No. 4, April 1998

Computation of Particle-Laden Turbulent Gas Flows Using Two Dispersion Models

X.-Q. Chen* and J. C. F. Pereira†
Instituto Superior Técnico, 1096 Lisbon Codex, Portugal

A hybrid Eulerian–Lagrangian model was used to study the solid particles, with a mean diameter of 49.3 μm and a standard deviation of 4.85 μm, dispersing from a turbulent wall-adjacent gaseous jet. Two Lagrangian particle dispersion models, the conventional stochastic discrete delta function model and a recently developed stochastic-probabilistic efficiency-enhanced dispersion (SPEED) model, were used to account for the particle dispersion induced by gas turbulence. The present work also investigated the effects of two different methods for determining the particle–eddy interaction time on the predicted particle property. Numerical predictions obtained with the different models using the conventional and modified particle–eddy interaction timescales were compared with each other and with experimental measurements. It was found that better agreement with experimental data could be achieved by using the modified particle–eddy interaction timescale. Moreover, it was demonstrated that the SPEED model could not only significantly improve the computational efficiency of the trajectory solver by a factor of 10 for the present flow considered but also yield smoother profiles and better agreement with the measurements than could the conventional Lagrangian stochastic discrete particle model.

Nomenclature

$C_{\varepsilon 1}$, $C_{\varepsilon 2}$	= standard k-ε model constants
$C_{\varepsilon 3}$	= model constant for two-phase turbulence modulation
C_μ	= k-ε model constant
C_σ	= model constant for the stochastic-probabilistic efficiency-enhanced dispersion (SPEED) model
$C_{\tau 1}$, $C_{\tau 2}$, $C_{\tau 3}$	= nonlinear k-ε model constants
D_p	= particle diameter
F_L	= lift force
f	= probability density function
f_p	= drag correction coefficient
G	= turbulence production
g	= gravity
k	= turbulent kinetic energy
l_e	= turbulent eddy length scale
P	= pressure
R_L	= Lagrangian autocorrelation function
S_k^p	= turbulence modulation
$S_{U_i}^p$	= two-phase momentum exchange
T_L	= Lagrangian integral timescale
t	= time
U	= mean velocity
u	= fluctuating velocity
$\overline{u_i u_j}$	= Reynolds stresses
V_{rel}	= relative velocity between the two phases
x	= Cartesian coordinate
δ_{ij}	= delta function, $= 1$ $(i = j)$ and $= 0$ $(i \neq j)$
ε	= dissipation rate of the turbulent kinetic energy
μ	= viscosity
ρ	= density
σ_k, σ_ε	= k-ε model constants
σ_p	= particle trajectory variance
τ_p	= particle relaxation time constant
$\forall$	= Eulerian control volume

Subscripts

eff	= effective
i, j	= coordinate components
int	= interaction
k	= coordinate component or kth particle size
m	= coordinate component
p	= particle phase
t	= turbulent

Introduction

DISCRETE Lagrangian trajectory models are currently used by many researchers for the simulation of particulate two-phase flows; see Refs. 1–3, etc. This is related to the fact that they are able to account for particle trajectory-crossing effects, particle–wall interactions, and particle–particle collisions, etc. Two recently completed reviews of numerical methods for predicting two-phase flows can be found in Elghobashi[4] and Crowe et al.[5]

Most existing Lagrangian stochastic models are based on the particle–eddy interaction model developed by Gosman and Ioannides.[6] In this model, the particles are assumed to randomly encounter a series of turbulent eddies, and the particle property determined in the trajectory computation solely represents one point in space. That is, a discrete delta function defines the spatial distribution. As a consequence, such a stochastic model often requires tracking a very large number of particle trajectories to achieve a stochastically invariant solution, even though it has been successfully used to predict a variety of dilute two-phase flows. For example, Mostafa et al.[7] reported that 100,000 particle trajectories were necessary for computing the monodispersed particle-laden jet. Adeniji-Fashola and Chen[8] achieved smoother particle properties' profiles using a total of 9000 computational particle trajectories for a confined particle-laden jet. Chang and Wu[9] found that a large number of 20,000 droplet trajectories were required to reach an invariant solution for the polydispersed hollow-cone spray. Furthermore, as many as 50,000 droplet trajectories were used by Berlemont et al.[10] to obtain the stochastically invariant solution for a polydispersed turbulent evaporating spray. In addition, Chen and Pereira[11] also found that a total of 10,000 droplet trajectories were necessary to achieve an invariant solution for the turbulent evaporating spray. Recently, Sato et al.[2] employed about 33,000 particle trajectories to compute a particle-laden planar turbulent jet. Obviously, the more particle trajectories are tracked, the more computer CPU time will be required for the Lagrangian solver. Such a large number of particle trajectories will further increase when three-dimensional two-phase flows are computed. As a result, computer CPU time will become unbearable if a large flow

Received July 24, 1997; revision received Dec. 6, 1997; accepted for publication Dec. 6, 1997.

*Senior Research Engineer, Department of Mechanical Engineering, Av. Rovisco Pais. E-mail: chen@navier.ist.utl.pt.

†Professor, Department of Mechanical Engineering, Av. Rovisco Pais. Member AIAA.

geometry results in a long particle residence time in the computational domain.

To overcome the deficiency in the existing conventional stochastic models, Chen and Pereira[12] developed an efficient Lagrangian trajectory model, stochastic-probabilistic efficiency-enhanced dispersion (SPEED), aimed at tracking a relatively small number of particle trajectories while offering a noise-free or noise-reduced computational solution. Such an efficient Lagrangian trajectory model was based on that of Litchford and Jeng,[13] but it differs from their model in that a more efficient approach was developed to determine the particle dispersion width induced by gas turbulence. The SPEED model was further improved by Chen and Pereira.[14, 15]

On the other hand, existing particle–eddy interaction models determine the interaction timescale as the minimum of an eddy lifetime and an eddy transit time. Recent analyses,[16–18] however, indicate that the existing eddy interaction models may predict that discrete heavy particles will disperse less rapidly in the long-time limit than will fluid particles. Evidently, this is contrary to the experimental observation that discrete particles may disperse faster than fluid particles. Their theoretical study further demonstrates that particle dispersion can be enhanced by modifying the method for determining the particle–eddy interaction time in the existing particle–eddy interaction models. It is found that, after the modification, the dispersion of discrete heavy particles in the long-time limit can be correctly predicted.

Therefore, the objective of this work is to further validate the SPEED model,[14] taking into account the recent analyses of Graham,[16] Graham and James,[17] and Graham[18] for a particle-laden turbulent gas flow with available detailed experimental measurements from Sato et al.[2] An early numerical study[19] has shown that the initial conditions play an important role in the accurate prediction of the particulate phase. Therefore, the experimental measurements are used to provide complete initial conditions for the two-phase flow computations. As a result, the influence of incomplete initial conditions on two-phase flow predictions, especially for the particulate phase, can be excluded. The effects of particle–eddy interaction timescales are also investigated using results from recent analyses.[16–18] The results of the SPEED model are compared with those of the conventional stochastic discrete delta function (SDDF) model. The computational efficiency of the SPEED model is assessed by making comparisons with that of the conventional SDDF model. In addition, the experimental measurements are used to evaluate the accuracy of the numerical predictions.

Two-Phase Flow Governing Equations

Gas Phase

Most of the existing turbulence models for the continuous phase in two-phase flow predictions are based on the standard k-ε model.[9, 20] However, such a turbulence closure model for the continuous phase cannot account for the effects of turbulence anisotropy on particle dispersion.[21] To overcome this deficiency, the nonlinear k-ε model[22] is used for the carrier gas phase to account for the anisotropy of turbulence. The governing equations for mass and momentum can be written tensorially as

$$\frac{\partial \rho U_j}{\partial x_j} = 0 \tag{1}$$

$$\frac{\partial \rho U_i U_j}{\partial x_j} = -\frac{\partial P}{\partial x_i} + \frac{\partial}{\partial x_j}\left[\mu \frac{\partial U_i}{\partial x_j} - \rho \overline{u_i u_j}\right] + S^p_{U_i} \tag{2}$$

The Reynolds stresses $\overline{u_i u_j}$ can be written tensorially as[23]

$$-\rho \overline{u_i u_j} = -\frac{2}{3}\rho k \delta_{ij} + \mu_t\left[\frac{\partial U_i}{\partial x_j} + \frac{\partial U_j}{\partial x_i}\right] - \rho \frac{k^3}{\varepsilon}\left[C_{\tau 1}\left(\frac{\partial U_i}{\partial x_k}\frac{\partial U_j}{\partial x_k}\right)^* + C_{\tau 2}\left(\frac{\partial U_i}{\partial x_k}\frac{\partial U_k}{\partial x_j} + \frac{\partial U_k}{\partial x_i}\frac{\partial U_j}{\partial x_k}\right)^* + C_{\tau 3}\left(\frac{\partial U_k}{\partial x_i}\frac{\partial U_k}{\partial x_j}\right)^*\right] \tag{3}$$

where the superscript $*$ represents the deviatory part[23]; for example, we have

$$\left[\frac{\partial U_i}{\partial x_k}\frac{\partial U_j}{\partial x_k}\right]^* = \left[\frac{\partial U_i}{\partial x_k}\frac{\partial U_j}{\partial x_k}\right] - \frac{2}{3}\left[\frac{\partial U_l}{\partial x_k}\frac{\partial U_l}{\partial x_k}\right]\delta_{ij} \tag{4}$$

The coefficients $C_{\tau 1}$, $C_{\tau 2}$, and $C_{\tau 3}$ in Eq. (3) are zero when the conventional standard linear k-ε model is used. In the framework of the k-ε model, the turbulent kinetic energy k is governed by

$$\frac{\partial \rho k U_j}{\partial x_j} = \frac{\partial}{\partial x_j}\left[\frac{\mu_{\text{eff}}}{\sigma_k}\frac{\partial k}{\partial x_j}\right] + (G - \rho\varepsilon) + S^p_k \tag{5}$$

and its dissipation rate ε is governed by

$$\frac{\partial \rho \varepsilon U_j}{\partial x_j} = \frac{\partial}{\partial x_j}\left[\frac{\mu_{\text{eff}}}{\sigma_\varepsilon}\frac{\partial \varepsilon}{\partial x_j}\right] + \frac{\varepsilon}{k}(C_{\varepsilon 1}G - C_{\varepsilon 2}\rho\varepsilon) + C_{\varepsilon 3}\frac{\varepsilon}{k}S^p_k \tag{6}$$

where the turbulence generation G is given by

$$G = -\rho \overline{u_i u_j}\frac{\partial U_i}{\partial x_j} \tag{7}$$

Note that the turbulence generation may be negative, especially in the course of numerical iteration when the nonlinear k-ε model is used. This is different from the standard k-ε model, where the generation is always positive. The model constants used in the foregoing equations are given as follows: (σ_k, σ_ε, C_μ, $C_{\tau 1}$, $C_{\tau 2}$, $C_{\tau 3}$, $C_{\varepsilon 1}$, $C_{\varepsilon 2}$, $C_{\varepsilon 3}$) = (1, 1.3, 0.09, 0.041, 0.014, −0.014, 1.45, 1.9, 1.1).

Particle Phase

In the framework of the Lagrangian formulation, the equation of motion for each representative particle size can be written

$$\frac{\mathrm{d}U_{pi}}{\mathrm{d}t} = \frac{\tilde{U}_i - U_{pi}}{\tau_p} f_p + \left[1 - \frac{\rho}{\rho_p}\right] g_i + F_{Li} \tag{8}$$

where the terms on the right-hand side denote the drag, gravity, and lift forces, respectively. The lift force is given (with no summation over j and $j \neq i$) by[24]

$$F_{Li} = \frac{3.0844}{\rho_p D_p}\sqrt{\rho\mu\left|\frac{\partial \tilde{U}_j}{\partial x_i}\right|}[\tilde{U}_j - U_{pj}] \tag{9}$$

In Eq. (8), $\tilde{U}_i$ represents the gas instantaneous velocity. The particle relaxation time constant τ_p is defined as

$$\tau_p = \frac{\rho_p D_p^2}{18\mu} \tag{10}$$

Following Clift and Gauvin,[25] the drag correction coefficient f_p is determined by

$$f_p = 1 + 0.15 Re_p^{0.687} \qquad \left(Re_p < 1 \times 10^3\right) \tag{11}$$

where the relative Reynolds number is defined as

$$Re_p = \frac{\rho V_{\text{rel}} D_p}{\mu} \tag{12}$$

The particle trajectories are computed by integrating the particle velocity; that is,

$$\frac{\mathrm{d}x_{pi}}{\mathrm{d}t} = \tilde{U}_{pi} \tag{13}$$

Due to the difficulty in determining the instantaneous gas velocity gradient, $\partial \tilde{U}_j / \partial x_i$, in Eq. (9), an approximate method[2] has been used for the determination of the gas velocity gradient along the particle trajectory.

Two-Phase Coupling Sources

In the present study, two-way coupling is accounted for by including the two-phase exchanges in momentum and kinetic energy. As no phase change occurs, the source term for the continuity equation is zero. The momentum exchange between the gas and particle phases is therefore determined as[26]

$$S^p_{U_i} = -\frac{1}{\forall}\sum \dot{N}_k\left[\Delta U_{pi} - \left(1 - \frac{\rho}{\rho_p}\right) g_i \Delta t - F_{Li}\Delta t\right]\frac{\pi}{6}\rho_p D_p^3 \tag{14}$$

where ΔU_{pi} is the velocity change of the particle residing in the control volume $\forall$ for a time interval Δt and the summation is made over

all particle trajectories across the control volume ∀. The turbulence modulation term is given by

$$S_k^p = \left\langle \tilde{U}_i S_{U_i}^p \right\rangle - \langle \tilde{U}_i \rangle \left\langle S_{U_i}^p \right\rangle \tag{15}$$

where $\langle\ \rangle$ denotes an ensemble average for all of the particle trajectories crossing the control volume ∀.

Two Particle Dispersion Models

Stochastic Discrete Delta Function Model

The conventional Lagrangian stochastic model[6] determines the instantaneous gas velocity by summing a fluctuating velocity u_i over the mean gas velocity of U_i, both of which are located at the current particle position. The fluctuating velocity is determined using the local kinetic energy k, under the assumption that the random distribution obeys the Gaussian probability density function (PDF). However, Chen and Pereira[21] found that such a dispersion model fails to predict the anisotropic effects of particle turbulent property. Therefore, the instantaneous gas velocity is presently obtained using the local Reynolds stresses [Eq. (3)] instead of the local kinetic energy k. The time during which a particle interacts with a turbulent eddy is determined by minimizing two timescales: an eddy lifetime and an eddy transit time. The eddy timescale is determined by

$$t_e = \sqrt{1.5} C_\mu^{0.75} (k/\varepsilon) = 0.21 (k/\varepsilon) \tag{16}$$

where C_μ is the model constant, as given before. The eddy transit time is given by

$$t_c = -\tau_p^* \ell n \left[1 - \frac{l_e}{V_{\text{rel}} \tau_p^*} \right] \tag{17}$$

where the eddy length scale is defined as

$$l_e = C_\mu^{0.75} (k^{1.5}/\varepsilon) \tag{18}$$

and τ_p^* is given by

$$\tau_p^* = \tau_p / f_p \tag{19}$$

Equation (17) was derived using the linearized particle's equation of motion without accounting for the lift force.[13] Strictly speaking, it is not valid for the present two-phase flow where the lift force has been included in Eq. (8). However, the lift force is usually very small, as compared with the other terms in the equation, owing to the small ratio of the gas to particle densities. Equation (17) is therefore still used for simplification in the present study. The modified particle–eddy interaction time[16] t_{int} is thus given as follows:

$$t_{\text{int}} = \begin{cases} T_f = 2t_e & \text{if} \quad V_{\text{rel}} < l_e / \tau_p^* \\ \min(T_{\max}, t_c) & \text{otherwise} \end{cases} \tag{20}$$

where $T_{\max}$ is set to some value, based on the turbulence structure parameter, to achieve a specified ratio of Lagrangian to Eulerian timescales. In the present study, a value of $2.8\, t_e$ was chosen as the limit of $T_{\max}$. According to the analysis,[16] the value of $T_{\max}$ should be about $3.16\, t_e$ as a result of the turbulence structure parameter equal to 1. It was, however, found that $T_{\max} = 2.8\, t_e$ gave slightly better agreement with the experimental measurements.[2] This was attributed to the ensuing constant of $C_\sigma = 1.5$ for the SPEED model, which was chosen slightly larger than unity, a limit value for tracer particles. In addition, it can be inferred that the criterion[16] was obtained under some simplified assumptions; it therefore may deviate from practical complex turbulent flows. The conventional particle–eddy interaction model[6] can be retrieved by setting $T_{\max} = T_f = t_e$.

Stochastic-Probabilistic Efficiency-Enhanced Dispersion Model

In conventional Lagrangian stochastic models, the particle trajectory obtained with Eq. (13) represents nothing but a single point in space. In other words, the discrete delta function model has been used for distributing the physical particles in space. Consequently, this model often requires tracking many individual particle trajectories to achieve a stochastically invariant solution. With the SPEED model, however, this deficiency can be surmounted and the computational efficiency can be enhanced. The SPEED model differs from the SDDF model in that it performs a probabilistic operation, in addition to the stochastic operation, at each Lagrangian time step along a particle trajectory. The probabilistic operation accounts for the spatial distribution of a particle in the physical space, based on a predetermined trajectory variance and an assumed probability density function. That is to say, a cloud of particles is tracked by using a representative size of the particles. Such a particle cloud has a mean trajectory determined by the conventional Lagrangian stochastic model and a spatial distribution governed by a predetermined probability density function. Following Chen and Pereira,[14] an ordinary differential equation can be derived to govern the trajectory variance. It reads tensorially as

$$\frac{\mathrm{d}\sigma_{pi}^2}{\mathrm{d}t} = 2\Omega_{pj} \delta_{ij} \bar{u}_j^2 \int_0^t R_{Lj}(\tau)\, \mathrm{d}\tau \tag{21}$$

where $R_{Li}(\tau)$ is a Lagrangian autocorrelation function, and Ω_{pj} denotes a relation for two-phase fluctuating velocity correlation. The repeated subscript j performs summation, and such a repeated summation practice is also valid for ensuing equations unless otherwise indicated. Introduction of this parameter in the trajectory-variance equation (21) is aimed at making it possible to compute the particle trajectory variance along the trajectory using the predicted gas flow Reynolds stresses $\bar{u}_j^2$; see Ref. 14 for details. Following Rizk and Elghobashi,[27] Ω_{pj} is determined (with no summation over i) by

$$\Omega_{pi} = C_\sigma \left[1 + 0.85 \frac{V_{\text{rel}}^2}{\bar{u}_i^2} \right]^{-0.5} \tag{22}$$

where $\bar{u}_i^2$ is the normal-stress component at the particle position. The new model constant is taken equal to 1.5, as suggested by Rizk and Elghobashi.[27] Our previous study[14] also demonstrated that such an expression gave better agreement with available measurements than an expression based on the Stokes number. For inhomogeneous turbulent flows, the Lagrangian autocorrelation function can be determined[20] by

$$R_{Li}(\tau) = \cos\left[\frac{\tau}{(m^2+1) T_{Lj}} \right] \exp\left[-\frac{\tau}{(m^2+1) T_{Lj}} \right] \delta_{ij} \tag{23}$$

where the loop parameter m is equal to unity, as suggested by Berlemont et al.,[20] who found that this value yielded good agreement with various experimental data. The integral timescale for each component in Eq. (23) is determined by[28]

$$T_{Li} = 0.235 \left(\bar{u}_i^2 / \varepsilon \right) \tag{24}$$

where $\bar{u}_i^2$ denotes the ith component of the normal stress, and no summation is performed. After introducing Eq. (23) into Eq. (21) and performing integration in part, Eq. (21) can be rewritten as

$$\frac{\mathrm{d}\sigma_{pi}^2}{\mathrm{d}t} = 2\Omega_{pj} \delta_{ij} \bar{u}_j^2 T_{Lj} \left\{ 1 - \exp\left(-\frac{t}{2T_{Lj}} \right) \times \left[\cos\left(\frac{t}{2T_{Lj}} \right) - \sin\left(\frac{t}{2T_{Lj}} \right) \right] \right\} \tag{25}$$

where the summation is made over the subscript j. Note that the Lagrangian advance step for integration is chosen in such a way that it is always smaller than 20% of the integral timescale to enhance numerical accuracy. Therefore, the right-hand side of Eq. (25) is always positive, as physically required. In both the conventional and efficient particle dispersion models, particles are assumed to interact with a series of turbulent eddies for a period of time determined as the minimum of an eddy lifetime and an eddy transit time. A recent analysis[16] indicates that particle dispersion can be enhanced by modifying the interaction timescale. Such a modification is aimed at overcoming the deficiency that the particle–eddy interaction timescale determined in conventional eddy interaction models always underpredicts the heavy particle dispersion compared with the tracer particle dispersion. As stated before, for the SPEED model, the trajectory determined with Eq. (13) only represents the

locus of the trajectory center at each Lagrangian advance step. Simultaneously, particle trajectory variances are determined with Eq. (25) to account for the dispersive effect induced by turbulence. To account for the anisotropy of turbulence, the particle–eddy interaction time, given by Eq. (16), is modified by averaging the two components of the integral timescale given by Eq. (24). Similarly, the eddy length scale is also modified by averaging the two components of the length scale, which are the product of the integral time and the squared root of the local normal stress.

Given a PDF, $f(x, y)$, the distribution of a physical particle in space can be determined. The ensemble-averaged particle property at an Eulerian control volume, $\Phi(x, y)$, can thus be obtained as[14]

$$\Phi(x, y) = \frac{\sum_{k=1}^{M} \dot{N}_k \Delta t_k \int_{x^l}^{x^u} \int_{y^l}^{y^u} \Phi_k(x_p, y_p) f_k(x, y)\, dx\, dy}{\sum_{k=1}^{M} \dot{N}_k \Delta t_k \int_{x^l}^{x^u} \int_{y^l}^{y^u} f_k(x, y)\, dx\, dy} \quad (26)$$

where the superscripts l and u denote the lower and upper integral boundaries, respectively, and the summation over k represents all of the particle sizes crossing the Eulerian control volume considered, with M being the total number of the particle trajectories. The term $\dot{N}_k$ in Eq. (26) denotes the particle number flow rate of the kth particle. Similarly, the distribution of two-way coupling sources can also be determined, except that the denominator of Eq. (26) is no longer required. This is because the coupling sources are calculated in terms of the absolute number of particles crossing the considered Eulerian control volume. Note that (x_p, y_p) in Eq. (26) represents the current particle position and that a prescribed PDF is required to determine the particle probability distribution in these equations. The Gaussian PDF is used for the present study. The detailed description of computing sources and ensembled properties can be found elsewhere.[14]

Computational Details

Figure 1 shows the experimental flow configuration of Sato et al.[2] The freestream gas has a velocity of 2 m/s. The solid particles are released from the wall-adjacent gas jet, which has a velocity of 10 m/s at the nozzle with a Reynolds number of 3.3×10^3. The transverse dimension is 100 mm, and the axial dimension for flow computation is taken to be 500 mm. The convective terms in the momentum equations are discretized using a third-order QUICK algorithm. Comparing the solutions obtained using grids of 82×72, 92×82, and 122×112 in the x and y directions, respectively, it was found that the grid of 92×82 gave almost the same solution as the grid of 122×112. The computational domain is therefore covered with the grid of 92×82. The initial conditions for Eulerian equations are obtained by interpolating the experimental measurements of Sato et al.[2] In the near-wall region, the conventional wall-function method is used to modify the momentum equations. That is, the tangential velocity at the wall-adjacent node is modified using the law of the wall to bridge the subviscose layer. Rizk and Elghobashi[27] found that the law of the wall could yield an error larger than 4% when the particle volume concentration is larger than 0.0005. However, the present particle volume concentration is typically smaller than 0.0005. Therefore the law-of-the-wall method is still used as the boundary wall modification in the present study. At the exit, the zero-gradient conditions are set for all the variables. The convergence criterion for the two-phase flow computations is that a residual of 5×10^{-3} is obtained after including two-way coupling sources in the gas flow equations. Regarding the dispersed phase, the experimental measurements at the inlet are used as input for initial Lagrangian conditions. The particle has a mean diameter of 49.3 μm and a standard deviation of 4.85 μm. The particle density is 2590 kg/m^3. The particle Stokes number ranges from 0.56 to 2.2 in the fully developed region[2] between $x = 150$ and 250 mm. The initial distribution of particle sizes is selected by summing over the mean diameter a random part that obeys a Gaussian distribution. That is, the particle sizes at the inlet are sampled by

$$D_p = 49.3 + 4.85\xi\ (\mu\text{m}) \quad (27)$$

where ξ is a Gaussian variable having zero mean and unity deviation. To achieve a stochastically invariant solution, a total number of 20,000 particle trajectories are tracked for the conventional SDDF model. However, a total number of 1000 particle trajectories are tracked for the SPEED model.

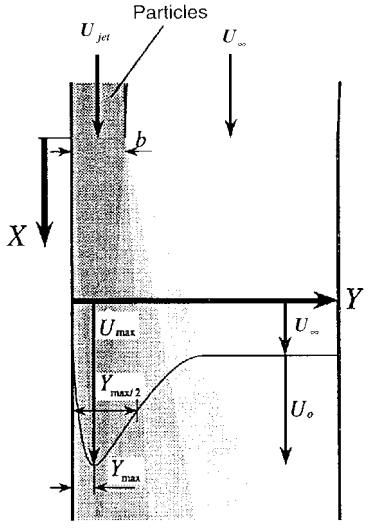

Fig. 1 Experimental setup of Sato et al.[2]

Results and Discussion

Gas Phase Flow Property

The gas axial mean velocity at three downstream stations is shown in Fig. 2, where the jet velocity ($U_{jet} = 10$ m/s) at the inlet is used for velocity normalization. The coordinates are normalized by the jet width $b = 5$ mm. Figure 2 shows that the nonlinear k-ε model yields slightly better predictions than the standard k-ε model, downstream of $x/b = 40$. This is obviously attributed to the nonlinear terms included in Eq. (4). The nonlinear terms redistribute the turbulence in each direction. The two components of the gas fluctuating velocity are shown in Figs. 3a and 3b. Of interest is the fact that the predictions for the standard and nonlinear k-ε models show an opposite tendency to agree with the measurements of Sato et al.[2] That is, the standard k-ε model better predicts the streamwise fluctuating velocity, whereas the nonlinear k-ε model better predicts the transverse fluctuating velocity. Therefore, it seems difficult to evaluate the two turbulence closure models. However, it can be clearly noted that the two components of the fluctuating velocity predicted with the standard k-ε model are almost isotropic, which is against the observed experimental measurements. In contrast, the nonlinear k-ε model has satisfactorily predicted the anisotropy of gas turbulence. This can be further clarified by Fig. 4, where the normalized difference between the two fluctuating velocity components is plotted. Note

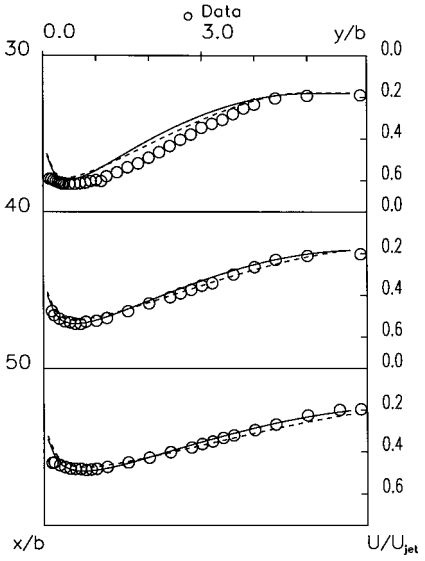

Fig. 2 Gas axial mean velocity obtained with the nonlinear (——) and standard (– – –) k-ε models.

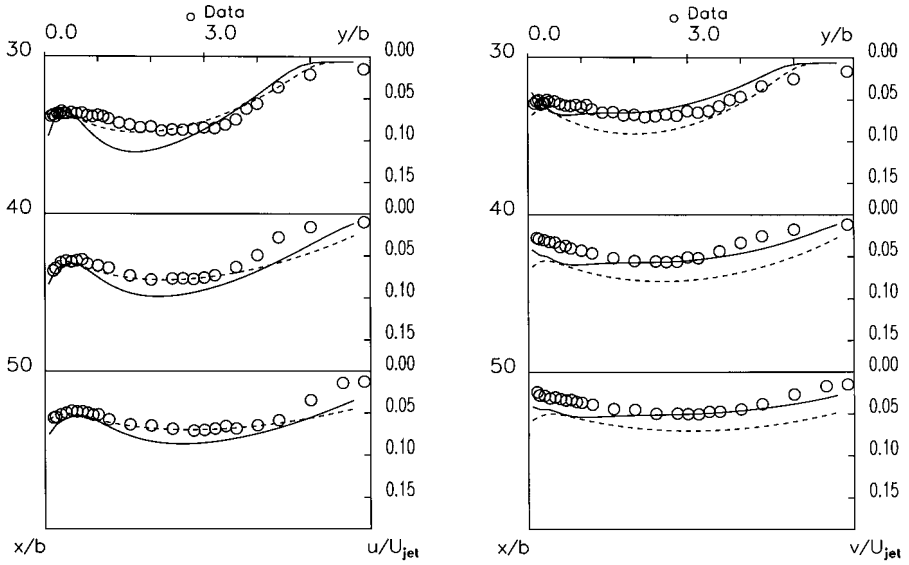

a) Axial component b) Transverse component

Fig. 3 Gas fluctuating velocities obtained with the nonlinear (——) and standard (– – –) k-ε models.

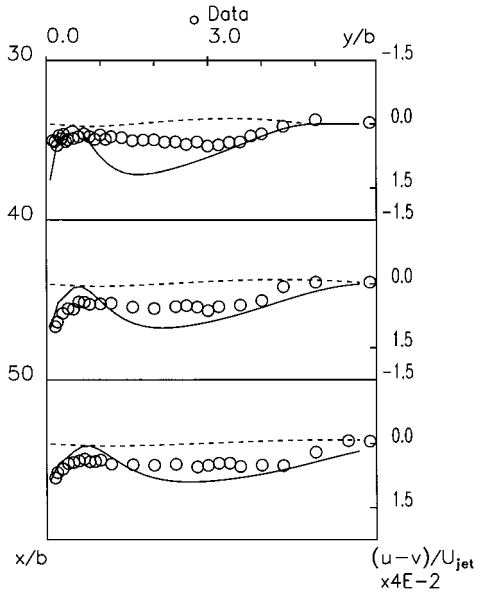

Fig. 4 Difference in two components of the gas fluctuating velocity obtained with the nonlinear (——) and standard (– – –) k-ε models.

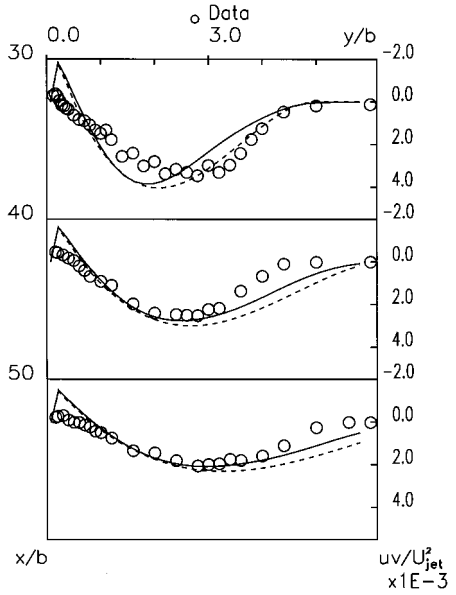

Fig. 5 Gas shear stress obtained with the nonlinear (——) and standard (– – –) k-ε models.

that, for clearer visualization, the experimental and numerical values have been arbitrarily amplified by a factor of 25 as indicated in the figure. Figure 4 clearly indicates that the standard k-ε model yields almost zero anisotropy of turbulence owing to the exclusion of the nonlinear terms present in the nonlinear k-ε model.

Figure 5 compares predictions for the gas shear-stress component. Here both the experimental and numerical values are amplified by a factor of 1000 to allow another clearer visualization. The comparison is also indicative of slight improvement with the nonlinear k-ε model. Note that the discontinuity of the shear stress near the wall is due to the wall function used to modify the momentum equations and turbulent generation for the node adjacent to the wall. The direct numerical simulation has shown that a large number of numerical grid nodes are required to resolve the near-wall region, which is computationally very expensive. As the present study used the nonlinear k-ε model for the gas flow, the wall-function method was employed. Such behavior also appeared in the results using the lower-Reynolds-number model.[2] Because the nonlinear k-ε model can account for the turbulence anisotropy, it is therefore used for the gas flow predictions in the ensuing two-phase flow predictions.

Effects of Interaction Timescales

As analyzed by Graham[16] and Graham and James,[17] the conventional particle–eddy interaction timescale, determined as the minimum of the eddy lifetime and eddy transit time, may underpredict the dispersion of the discrete heavy particles as compared with that of the fluid particles. Their analysis shows, however, that by adequately modifying the conventional particle–eddy interaction time the particle dispersion in the long-time limit can be correctly predicted. By setting $T_{\max}$ to some value larger or smaller than the eddy lifetime, adequate particle dispersion can be achieved. As explained before, $T_{\max} = 2.8t_e$ was chosen for the present particle-laden turbulent gas flow. To understand the effects of the interaction timescale on particle dispersion, two different timescales are used to account for the particle–eddy interaction: one determined by Shuen et al.,[29] which is a slight modification on the model of Gosman and Ioannides,[6] and another determined by Graham.[16]

Figures 6a and 6b show the numerical predictions of the particle fluctuating velocity using two different particle–eddy interaction timescales. Here SDDF-A and SDDF-B represent the predictions with the conventional discrete delta function model using the modified particle–eddy interaction timescale,[16] i.e., Eq. (20), and the standard interaction timescale,[27] respectively. Of particular note is that, to achieve a stochastically invariant solution, 20,000 particle trajectories have been tracked for these SDDF model predictions. It can be seen that the modified particle–eddy interaction timescale leads to larger particle dispersion and yields better agreement with the experimental measurements. Such enhanced particle dispersion

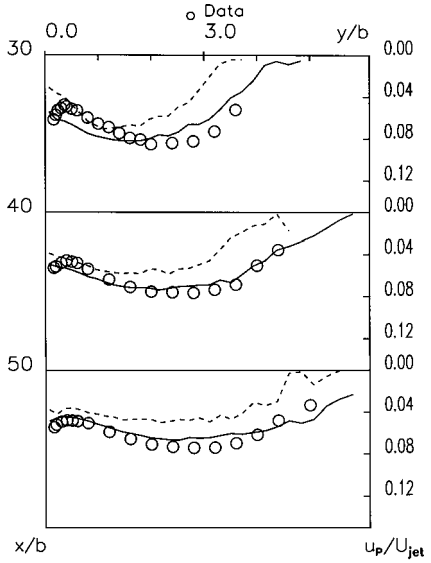

a) Axial

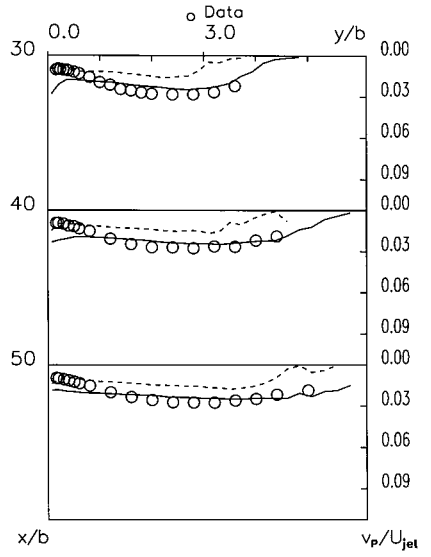

b) Transverse

Fig. 6 Particle fluctuating velocities obtained with the SDDF model (——, modified interaction timescale, and – – –, standard interaction timescale) using 2×10^4 trajectories.

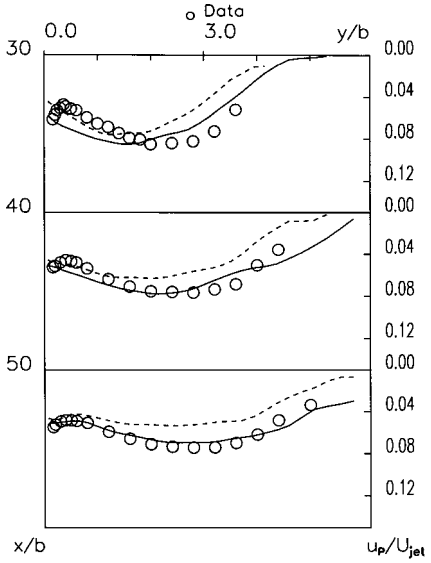

a) Axial

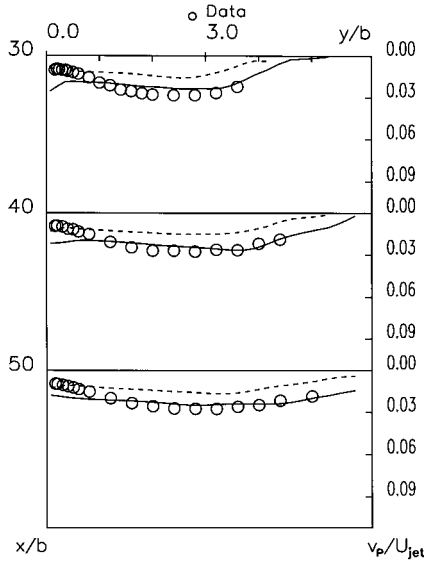

b) Transverse

Fig. 7 Particle fluctuating velocities obtained with the SPEED model (——, modified interaction timescale, and – – –, standard interaction timescale) using 10^3 trajectories.

is the direct result of the chosen time limit T_{max} in Eq. (20). For the predictions obtained with the conventional particle–eddy interaction timescale (SDDF-B), there exist some zigzag changes in the fluctuating velocity profiles on the outer edge of the jet. This is because the particles were released from the wall-adjacent jet and were dispersed gradually outwards under the gas turbulence. As a result, fewer particles are present in the region away from the wall than close to the wall, and ensemble-averaged particle velocities cannot be reliably obtained on the jet edge. This can be clearly observed in the SDDF-B predictions using the conventional particle–eddy interaction timescale; see the dashed lines in Figs. 6a and 6b. However, such zigzag changes have been substantially reduced in the SDDF-A predictions. This is because the enhanced particle–eddy interaction timescale has been used in the SDDF-A predictions. Obviously, the direct result of the enhanced particle dispersion is that more particles can be present in the jet outer edge. This leads to relatively reliable statistics of the particle fluctuating velocities on the plotted jet edge. For this reason, the particle fluctuating velocity profiles obtained with the modified timescale (SDDF-A) are much smoother than those obtained with the standard timescale (SDDF-B).

Figures 7a and 7b compare the numerical predictions obtained with the SPEED model using the two interaction timescales. Once again, SPEED-A and SPEED-B correspond to the predictions obtained with the SPEED model using the modified and standard particle–eddy interaction timescales, respectively. It should be stressed here that only 1000 particle trajectories were tracked in these SPEED model predictions. A similar trend is observed in the predicted particle fluctuating velocities. However, much smoother profiles are achieved with the two versions of the SPEED model no matter what interaction timescale has been used. This is attributed to the probabilistic computation included in the SPEED model. The probabilistic computation distributes spatially the physical particles at each Lagrangian time step. As a result, smoother profiles can be obtained even though a much smaller number of particles are tracked for the SPEED model. This is in striking contrast to the SDDF model in which Lagrangian computations at each time step only represent a single point in space. It is for this reason that some zigzag changes are still present in the SDDF predictions, regardless of the larger number of particle trajectories (20,000) tracked for the model. Evidently, the comparisons in Fig. 7 have demonstrated that the predictions obtained with the modified timescale agree more satisfactorily with the experimental measurements. This is also indicative of the success in modifying the particle–eddy interaction timescale for the SPEED model. The modification does bring the model predictions toward better agreement with the measurements,[2] owing to the enhanced particle dispersion.

Computational Efficiency and Accuracy

In this section, the computational efficiency and accuracy are evaluated in terms of computer CPU time and agreement with experimental measurements. The previous comparisons have demonstrated that the modified eddy interaction timescale improves both the SDDF and SPEED predictions, yielding better agreement with the experimental measurements. Therefore, the following model assessment is based upon the modified eddy interaction timescale. Figures 8a and 8b compare the predicted particle velocity fluctuations obtained with the conventional (SDDF) and efficient (SPEED) models, with the aim of assessing the computational efficiency and accuracy of the two particle dispersion models. Note that there exists a large difference in the number of particle trajectories between the SDDF model (20,000 trajectories) and SPEED model (1000 trajectories) and that the interaction timescales used in these two model predictions are based upon the modified one.[16] Figures 8a and 8b clarify that the SPEED model yields slightly better and smoother predictions than the SDDF model, even though it computes only 5% (the ratio of SPEED model trajectories to SDDF model trajectories) of the total number of particle trajectories tracked with the SDDF model. This indicates that the SPEED model is really capable of adequately accounting for the distribution of the physical particles in space to achieve the smooth profiles and improves the numerical predictions as a result. The computational efficiency of the two dispersion models can be evaluated in terms of their CPU times. It is found that the ratio of the computer CPU time required by SPEED to that by SDDF is about 10%. This evidently illustrates that the stochastic-probabilistic model does substantially enhance computational efficiency.

In the following comparisons, the particle axial mean velocity, shear stress, and volume concentration were also obtained with the SDDF and SPEED models using the modified interaction timescale.[16] Displayed in Fig. 9 is the particle axial mean velocity obtained with the two dispersion models. There is a very slight discrepancy in the predicted particle axial mean velocity, regardless of the large difference in the number of particle trajectories between the two dispersion models. This is because the particle mean velocity is not sensitive to the number of particle trajectories.[11] The particle shear-stress predictions with the SDDF and SPEED models are compared in Fig. 10, where the experimental and numerical values have been arbitrarily amplified by a factor of 250. It is evident that the SPEED model predictions yield much smoother profiles than the SDDF model. This is obviously attributable to the probabilistic computation carried out in the SPEED model, which distributes the

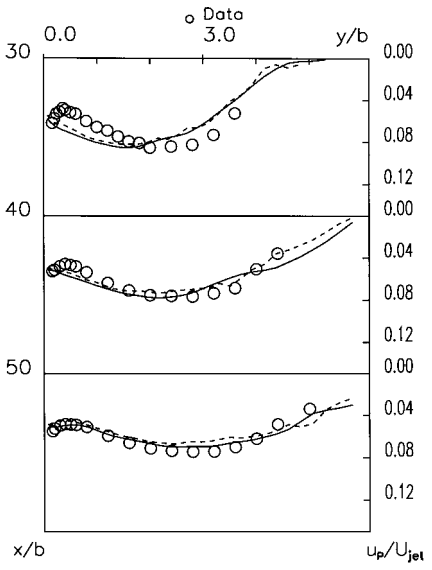

a) Axial

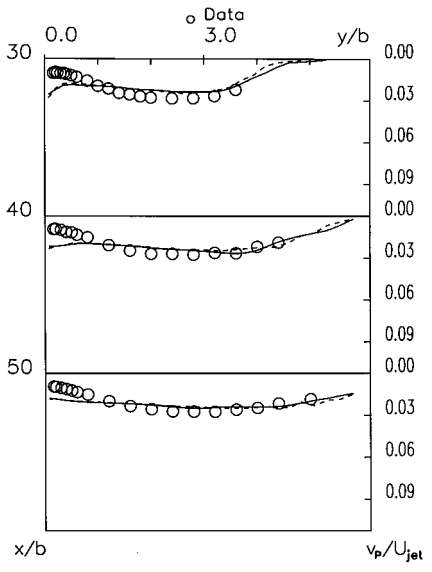

b) Transverse

Fig. 8 Particle fluctuating velocities obtained with the SPEED model (——) using 10^3 trajectories and the SDDF model (– – –) using 2×10^4 trajectories based on the modified interaction timescale.

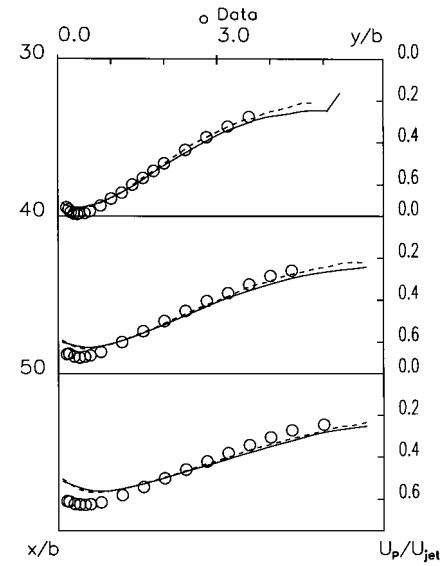

Fig. 9 Particle axial mean velocities obtained with the SPEED model (——) using 10^3 trajectories and the SDDF model (– – –) using 2×10^4 trajectories based on the modified interaction timescale.

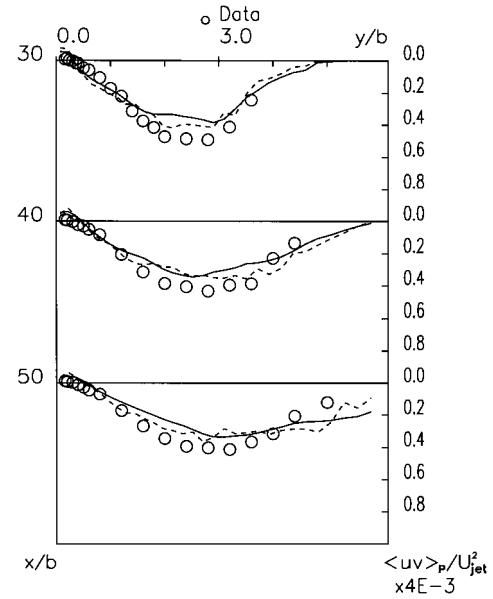

Fig. 10 Particle shear stress obtained with the SPEED model (——) using 10^3 trajectories and the SDDF model (– – –) using 2×10^4 trajectories based on the modified interaction timescale.

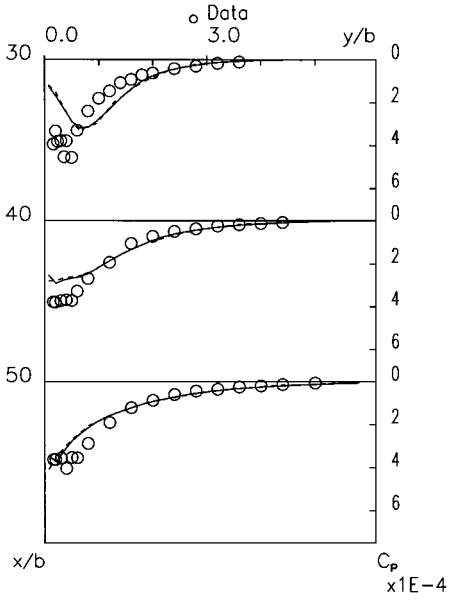

Fig. 11 Particle volume concentration obtained with the SPEED model (——) using 10^3 trajectories and the SDDF model (– – –) using 2×10^4 trajectories based on the modified interaction timescale.

physical particles in space and smooths the profiles. Figure 10 also shows that the particle shear stress is a sensitive property for prediction. With a SDDF model, a larger number of particle trajectories are required if we want to reach smoother shear-stress profiles.

Figure 11 finally plots the profiles of the particle volume concentration obtained with the SPEED and SDDF models. Here the experimental and numerical values have been amplified by a factor of 10,000 for easy observation. The two dispersion models give very close predictions. The profiles are very smooth for both model predictions. It has been found that the particle volume concentration is not very sensitive to the number of particle trajectories for the present particle-laden turbulent gas flow. This is probably because the particles are nearly monosized (about 50 μm) in the present study and the particle volume concentration is computed using the absolute total number of particles within the Eulerian control volume in question.

Concluding Remarks

Solid particle dispersion in a turbulent wall jet has been investigated numerically using the Eulerian–Lagrangian hybrid model. Detailed experimental measurements were used as the initial conditions, thus excluding the effects of the incomplete initial conditions on two-phase flow predictions. The present numerical results were compared with the experimental measurements of Sato et al.[2] It was found that the nonlinear k-ε model could predict the anisotropy of gas turbulence better than the linear k-ε model could, that the particle dispersion could be enhanced by modifying the particle–eddy interaction timescale, and that the efficient Lagrangian trajectory model could substantially improve computational efficiency as compared with the conventional Lagrangian stochastic model. Results also indicated that, for the present particle-laden turbulent gas flow, using the modified particle–eddy interaction timescale the prediction of particle velocity fluctuations could be improved with the SPEED model as compared with the conventional dispersion model.

Acknowledgment

The first author gratefully acknowledges the research grant of the Portuguese foundation Junta Nacional de Investigação Científica e Tecnológica under the program of Orçamento Programático.

References

[1]Tsuji, Y., "Discrete Particle Simulation of Gas-Solid Flows," *KONA Power Part*, Vol. 11, No. 5, 1993, pp. 57–68.

[2]Sato, Y., Hishida, K., and Maeda, M., "Effect of Dispersed Phase on Modification of Turbulent Flow in a Wall Jet," *Journal of Fluids Engineering*, Vol. 118, June 1996, pp. 307–315.

[3]Chen, X.-Q., Freek, C., and Pereira, J. C. F., "Experimental and Numerical Study of a Water Spray in the Wake of an Axisymmetric Bluff Body," *Experimental Thermal and Fluid Science*, Vol. 13, No. 1, 1996, pp. 129–141.

[4]Elghobashi, S. E., "On Predicting Particle-Laden Turbulent Flows," *Applied Scientific Research*, Vol. 52, 1994, pp. 309–329.

[5]Crowe, C. T., Troutt, T. R., and Chung, J. N., "Numerical Models for Two-Phase Turbulent Flows," *Annual Review of Fluid Mechanics*, Vol. 28, 1996, pp. 11–43.

[6]Gosman, A. D., and Ioannides, E., "Aspects of Computer Simulation of Liquid-Fuelled Combustors," AIAA Paper 81-0323, June 1981.

[7]Mostafa, A. A., Mongia, H. C., McDonell, V. G., and Samuelsen, G. S., "Evolution of Particle-Laden Jet Flows: A Theoretical and Experimental Study," *AIAA Journal*, Vol. 27, No. 2, 1989, pp. 167–183.

[8]Adeniji-Fashola, A., and Chen, C. P., "Modelling of Confined Turbulent Fluid-Particle Flows Using Eulerian and Lagrangian Schemes," *International Journal of Heat and Mass Transfer*, Vol. 33, No. 4, 1990, pp. 691–701.

[9]Chang, K.-C., and Wu, W.-J., "Sensitivity Study on Monte Carlo Solution Procedure of Two-Phase Turbulent Flows," *Numerical Heat Transfer*, Vol. 25, No. 2, 1994, pp. 223–244.

[10]Berlemont, A., Grancher, M. S., and Gouesbet, G., "Comparison Between Experiments and Simulations for the Two-Way Coupling Between Vaporising Droplets and Turbulent Round Jet," *Gas-Particle Flows*, Vol. 228, American Society of Mechanical Engineers, New York, 1995, pp. 279–287.

[11]Chen, X.-Q., and Pereira, J. C. F., "Computation of Turbulent Evaporating Sprays with Well-Specified Measurements: A Sensitivity Study on Droplet Properties," *International Journal of Heat and Mass Transfer*, Vol. 39, No. 3, 1996, pp. 441–454.

[12]Chen, X.-Q., and Pereira, J. C. F., "Stochastic-Probabilistic Efficiency Enhanced Dispersion Modeling of Turbulent Polydispersed Sprays," *Journal of Propulsion and Power*, Vol. 12, No. 4, 1996, pp. 760–769.

[13]Litchford, R. J., and Jeng, S.-M., "Efficient Statistical Transport Model for Turbulent Particle Dispersion in Sprays," *AIAA Journal*, Vol. 29, No. 9, 1991, pp. 1443–1451.

[14]Chen, X.-Q., and Pereira, J. C. F., "Efficient Computation of Particle Dispersion in Dispersed Turbulent Flows with a Stochastic-Probabilistic Model," *International Journal of Heat and Mass Transfer*, Vol. 40, No. 8, 1997, pp. 1727–1741.

[15]Chen, X.-Q., and Pereira, J. C. F., "Computation of Particle Dispersion in Turbulent Liquid Flows Using an Efficient Lagrangian Trajectory Model," *International Journal of Numerical Methods in Fluids* (to be published).

[16]Graham, D. I., "On the Inertial Effect in Eddy Interaction Models," *International Journal of Multiphase Flow*, Vol. 22, No. 1, 1996, pp. 177–184.

[17]Graham, D. I., and James, P. W., "Turbulent Dispersion of Particles Using Eddy Interaction Models," *International Journal of Multiphase Flow*, Vol. 22, No. 1, 1996, pp. 157–175.

[18]Graham, D. I., "Dispersion of Initially-Static and Initially-Excited Particles in a Turbulent Fluid Flow," *International Journal of Multiphase Flow*, Vol. 22, No. 5, 1996, pp. 1005–1021.

[19]Solomon, A. S. P., Shuen, J. S., Zhang, Q.-F., and Faeth, G. M., "Structure of Nonevaporating Sprays, Part I: Initial Conditions and Mean Properties," *AIAA Journal*, Vol. 23, No. 10, 1985, pp. 1548–1555.

[20]Berlemont, A., Desjonqueres, P., and Gouesbet, G., "Particle Lagrangian Simulation in Turbulent Flows," *International Journal of Multiphase Flow*, Vol. 16, No. 1, 1990, pp. 19–34.

[21]Chen, X.-Q., and Pereira, J. C. F., "Prediction of Evaporating Spray in Anisotropically Turbulent Gas Flow," *Numerical Heat Transfer*, Vol. 27, No. 2, 1995, pp. 143–162.

[22]Speziale, C. G., "On Non-Linear k-l and k-ε Models of Turbulence," *Journal of Fluid Mechanics*, Vol. 178, May 1987, pp. 459–475.

[23]Lien, F. S., and Leschziner, M. A., "Assessment of Turbulence-Transport Models Including Nonlinear RNG Eddy-Viscosity Formulation and Second-Moment Closure for Flow over a Backward-Facing Step," *Computers and Fluids*, Vol. 23, No. 8, 1994, pp. 983–1004.

[24]Saffman, P. G., "The Lift on a Small Sphere in a Slow Shear Flow," *Journal of Fluid Mechanics*, Vol. 22, Pt. 2, 1965, pp. 385–400.

[25]Clift, R., and Gauvin, W. H., "Motion of Entrained Particles in Gas Streams," *Canadian Journal of Chemical Engineering*, Vol. 49, Aug. 1971, pp. 439–448.

[26]Durst, F., Milojevic, D., and Schonung, B., "Eulerian and Lagrangian Prediction of Particulate Two-Phase Flows: A Numerical Study," *Applied Mathematical Modelling*, Vol. 8, April 1984, pp. 101–115.

[27]Rizk, M. A., and Elghobashi, S. E., "A Two-Equation Turbulence Model for Dispersed Dilute Confined Two-Phase Flow," *International Journal of Multiphase Flow*, Vol. 15, No. 1, 1989, pp. 119–133.

[28]Lu, Q. Q., Fontaine, J. R., and Aubertin, G., "Particle Dispersion in Shear Flows," *Aerosol Science and Technology*, Vol. 18, 1993, pp. 85–99.

[29]Shuen, J.-S., Solomon, A. S. P., Zhang, Q.-F., and Faeth, G. M., "Structure of Particle-Laden Jets: Measurements and Predictions," *AIAA Journal*, Vol. 23, No. 3, 1985, pp. 396–404.

G. M. Faeth
Associate Editor